Chemical Science

[NiIII(OMe)]-Mediated Reductive Activation of CO2 Affording a Ni(κ1-OCO) Complex

Journal:	*Chemical Science*
Manuscript ID	SC-EDG-12-2015-004652.R1
Article Type:	Edge Article
Date Submitted by the Author:	15-Feb-2016
Complete List of Authors:	Liaw, Wen-Feng; National Tsing Hua University, Department of Chemistry Lu, Tsai-Te; Chung Yuan Christian University, Chemistry Chiou, Tzung-Wen; National Tsing Hua University Tseng, Yen-Ming; Nationa Tsing Hua University, Chemistry Weng, Tsu-Chien; Stanford Synchrotron Radiation Lightsource, SLAC National Accelorator Laboratory, Sokaras, Dimosthenis; SLAC National Accelerator Laboratory Ho, Wei-Jie ; National Tsing Hua Unviserty Kuo, Ting-Shen; National Taiwan Normal University, Chemsitry Jang, Ling–Yun; National Synchrotron Radiation Research Center, Lee, Jyh-Fu; National Synchrotron Radiation Research Center, Experimental Facility Division

Chemical Science

ARTICLE

[Ni^{III}(OMe)]-Mediated Reductive Activation of CO_2 Affording a Ni(κ^1-OCO) Complex

Received 00th January 20xx,
Accepted 00th January 20xx

DOI: 10.1039/x0xx00000x

www.rsc.org/

Tzung-Wen Chiou,*[a] Yen-Ming Tseng,[a] Tsai-Te Lu,[b] Tsu-Chien Weng,[c] Dimosthenes Sokaras,[c] Wei-Chieh Ho,[a] Ting-Shen Kuo,[d] Ling-Yun Jang,[e] Jyh-Fu Lee,[e] Wen-Feng Liaw*[a]

Carbon dioxide has been expected to be employed as inexpensive and potential feedstock of C_1 sources for mass production of valuable chemicals and fuel. Versatile chemical transformations of CO_2, i.e. insertion of CO_2 producing bicarbonate/acetate/formate, cleavage of CO_2 yielding μ-CO/μ-oxo transition-metal complexes, and electrocatalytic reduction of CO_2 affording CO/HCOOH/CH_3OH/CH_4/C_2H_4/oxalate were well documented. Herein, we report a novel pathway for the reductive activation of CO_2 by complex [Ni^{III}(OMe)($P(C_6H_3$-3-$SiMe_3$-2-$S)_3$)]$^-$ yielding complex [Ni^{III}(κ^1-$OCO^{\bullet-}$)($P(C_6H_3$-3-$SiMe_3$-2-$S)_3$)]$^-$. Formation of this unusual Ni^{III}(κ^1-OCO•$^-$) complex was characterized by single-crystal X-ray diffraction, EPR, IR, SQUID, Ni/S K-edge X-ray absorption spectroscopy, and Ni valence-to-core X-ray emission spectroscopy. The inertness of analogous complexes [Ni^{III}(SPh)], [Ni^{II}(CO)], and [Ni^{II}(N_2H_4)] toward CO_2, in contrast, demonstrates that the ionic [Ni^{III}(OMe)] core attracts the binding of weak σ-donor CO_2 and triggers the subsequent reduction of CO_2 by the nucleophilic [OMe]$^-$ in the immediate vicinity. This metal-ligand cooperative activation of CO_2 may open a novel pathway promoting the subsequent incorporation of CO_2 in the buildup of functionalized products.

Introduction

Carbon dioxide, the waste from human activity embodying the nature of highly thermodynamic stability and chemical inertness, has been expected to be employed as inexpensive and potential feedstock of C_1 sources for the regeneration of valuable chemicals and fuel.[1,2] Nature developed carbon monoxide dehydrogenase (CODH) to harbor a Ni-Fe cluster for the reversible interconversion between CO_2 and CO.[3-5] To gain the insight into the mechanism for the conversion of CO_2 to CO in CODH, several Ni-CO_2 adducts derived from reaction of low-valent Ni complex and CO_2 were reported.[6-9] Direct electrochemical reduction of CO_2 affords oxalate, carbon monoxide, formic acid, methanol, methane, and ethylene.[10] To gain the insight to the transformation of CO_2 at a molecular level, the chemistry for the activation of CO_2 via nucleophilic attack/interaction on the polarized C center, in addition to the reduction of the coordinated CO_2 ligand by low-valence transition metal complexes, has grown explosively over the past years.[11] The versatile chemical transformations of CO_2, i.e. insertion of CO_2 producing bicarbonate/acetate/formate,[12-18] cleavage of CO_2 yielding μ-CO/μ-oxo transition-metal complexes,[19-23] reduction of CO_2 affording CO/HCOOH/CH_3OH/CH_4/C_2H_4/C_2H_6/methylene, and electrocatalysis of CO_2 converting into oxalate, were well documented.[24-26] Direct electrochemical reduction or electrocatalytic transformation of CO_2 for mass production of valuable chemicals and fuel, however, relies on the consumption of sustainable electric potential energy. Here we show a novel pathway for the reductive activation of CO_2 by mononuclear Ni(III) complex [Ni^{III}(OMe)($P(C_6H_3$-3-$SiMe_3$-2-$S)_3$)]$^-$.[27] This [Ni^{III}-(OMe)]-mediated reduction of CO_2 yields complex Ni^{III}(κ^1-OCO•$^-$) evidenced by single-crystal X-ray diffraction, EPR, SQUID, Ni/S K-edge X-ray absorption spectroscopy, IR and Ni valence-to-core X-ray emission spectroscopy. The ionic [Ni^{III}(OMe)] core provides a kinetic pathway to induce the binding of CO_2 and trigger the subsequent reduction of CO_2 by the nucleophilic [OMe]$^-$ in the immediate vicinity. The covalent [Ni^{III}(SPh)] core as well as Ni(II) center in complexes [Ni^{II}(L)($P(C_6H_3$-3-$SiMe_3$-2-$S)_3$)]$^-$ (L = CO or N_2H_4), in contrast, are inert toward CO_2.[28]

Results and discussion

Synthesis and characterization of nickel κ^1-OCO complex

Upon CO_2(g) bubbled into the thermally stable [Ni^{III}(OMe)(PS_3)]$^-$ (**1**) (PS_3 = $P(C_6H_3$-3-$SiMe_3$-2-$S)_3$) in THF,[27] a pronounced color change from blue green to yellow green occurred to yield the O-bound κ^1-CO_2 complex [Ni(κ^1-OCO)(PS_3)]$^-$ (**2**), instead of complexes [Ni(OC(O)OCH_3)-(PS_3)]$^-$ or [Ni(OC(O)H)(PS_3)]$^-$ via the classical insertion or β–H migration mechanisms (Scheme 1a).[9,12-16]

Accompanied formation of [•OMe] in the reaction described above was corroborated using spin-trapping reagent DMPO (Supplementary Information (SI) Figure S1).[29] IR ν_{OCO} stretching peak at 2177 cm^{-1} (KBr) (ν_{OCO}: 2226 cm^{-1} in THF) exhibited by complex **2** supports the formation of [Ni(κ^1-OCO)(PS_3)]$^-$, which is consistent with the isotopic shift of IR υ_{OCO} stretching peak to 2117 cm^{-1} (KBr) observed in the $^{13}CO_2$ labeling experiment (SI Figure S2). The conversion of complex **1** to complex **2** under CO_2 atmosphere was also monitored by UV-vis spectrometry, the intense bands at 419 and 605 nm disappeared with simultaneous formation of absorption bands at 425 and 610 nm (THF) (SI Figure S3). The green needle crystals of complex **2** were isolated when complex **2** was

[a] Department of Chemistry, National Tsing Hua University, Hsinchu, 30013, Taiwan. E-mail: d9623817@oz.nthu.edu.tw (T.-W.C); wfliaw@mx.nthu.edu.tw (W.-F.L)
[b] Department of Chemistry, Chung Yuan Christian University, Taoyuan, 32023, Taiwan
[c] SLAC National Accelerator Laboratory, Menlo Park, CA 94025, USA
[d] Department of Chemistry, National Taiwan Normal University, Taipei, 10610, Taiwan
[e] National Synchrotron Radiation Research Center, Hsinchu, 30013, Taiwan
Electronic Supplementary Information (ESI) available: [details of any supplementary information available should be included here]. See DOI: 10.1039/x0xx00000x

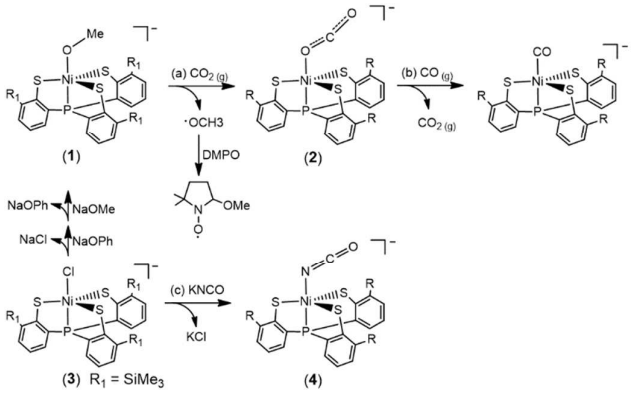

Scheme 1

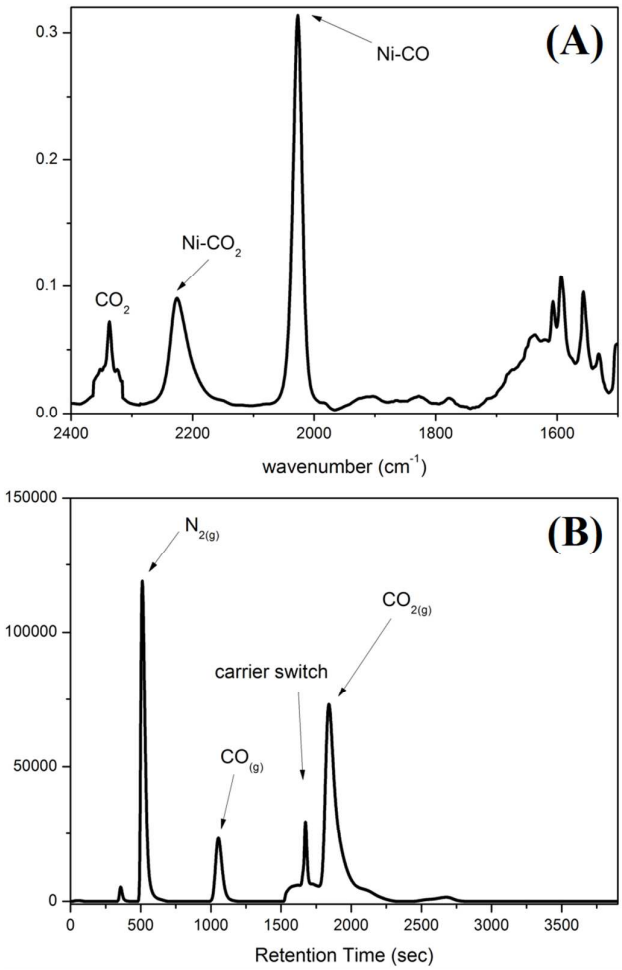

Figure 1. (**A**) IR spectra for the transformation of complex **2** to $[Ni^{II}(CO)(PS_3)]^-$ in THF. The decrease of the intensity of the IR υ_{CO2} peak at 2226 cm^{-1} exhibited by complex **2** with simultaneous formation of IR υ_{CO} peak at 2027 cm^{-1} indicated the formation of complex $[Ni^{II}(CO)(PS_3)]^-$. (**B**) GC chromatogram, derived from the sample collected from the headspace of the tube containing the reaction solution of complex **2** and $CO_{(g)}$, indicated the release of CO_2(g) during the transformation of complex **2** to $[Ni^{II}(CO)(PS_3)]^-$.

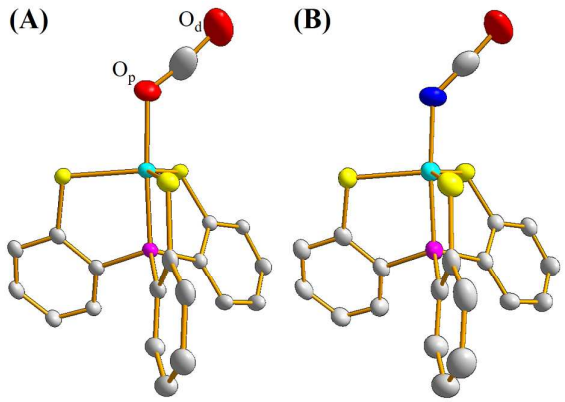

Figure 2. ORTEP drawing schemes of (A) complex **2** and (B) complex **4** with thermal ellipsoids drawn at 50% probability level. The Ni, P, S, O, N, and C atoms are shown as light blue, purple, yellow, red, blue, and white ellipsoids. H atom and TMS group are omitted for clarity. Selected bond distances (Å) and angles (°) for complex 2: Ni–O_p 2.028(3); Ni–P 2.122(1); Ni–S 2.221(1), 2.287(1), and 2.285(1); O_p–C 1.132(6); O_d–C 1.240(7); O–Ni–P 176.2(1); Ni–O–C 127.0(4); O_p–C–O_d 171.7(7). Selected bond distances (Å) and angles (°) for complex 4: Ni–N 1.933(2); Ni–P 2.120(1); Ni–S 2.226(1), 2.286(1), and 2.291(1); O–C 1.200(3); N–C 1.181(3); N–Ni–P 175.0(1); Ni–N–C 135.1(2); O–C–N 177.2(3).

recrystallized from THF-diethyl ether at room temperature. As shown in Scheme 1b, treatment of complex **2** with $CO_{(g)}$ led to the formation of the reported complex $[Ni^{II}(CO)(PS_3)]^-$ accompanied by the release of CO_2(g) characterized by IR and GC (Figure 1).[28]

To contrast complex **2** containing a $[Ni^{III}:CO_2^{\bullet-}]$ or $[Ni^{II}:CO_2]$ center, complex $[Ni^{III}(NCO)(PS_3)]^-$ (**4**) was synthesized via reaction of $[Ni(Cl)(PS_3)]^-$ (**3**) and [K][NCO] to mimic the isolobal $[Ni^{III}:CO_2]$ (Scheme 1c). Figure 2 displays ORTEP plots of complexes **2** and **4**, with the selected bond distances and angles given in the caption. The strain effect of the chelating ligand ($[PS_3]^{3-}$) in the coordination sphere of complexes **2** and **4** explains the Ni in a distorted trigonal bipyramidal geometry with three thiolates locating equatorial positions and the phosphorus occupying an axial position trans to [OCO] and [NCO] ligands. In contrast to the linear N–C–O (177.2(3)°) bond observed in complex **4**, complex **2** displays the bent O–C–O bond with the bond angle of 171.7(7)°. Compared to the similar O–C and N–C bond distances of 1.200(3) and 1.181(3) Å in complex **4**, the dramatic difference (~ 0.1 Å) of O–C bond lengths, 1.132(6) v.s. 1.240(7) Å, found in complex **2**, moreover, implicates the polarization of CO_2 via reductive activation affording a $[Ni^{III}:CO_2^{\bullet-}]$ species.[22, 30-31] A similar polarization of CO_2 was reported in the O-bound κ^1-CO_2 coordinated complex $[((^{Ad}ArO)_3tacn)\text{-}U^{IV}(CO_2^{\bullet-})]$ ($(^{Ad}ArOH)_3tacn$ = 1,4,7-tris(3-adamantyl-5-tert-butyl-2-hydroxybenzyl)-1,4,7-triazacyclononane), O–C = 1.122 (4) and 1.277 (7) Å, with the linear U-O-C and O-C-O bonds stabilized by the sterically encumbering ligand framework.[30-31] Besides, complex **2** displays the significantly longer Ni–O bond distance (2.028(3) Å) than those observed in complexes $[Ni^{II}(L)(pyN_2^{Me2})]^{1-}$ (1.857(5) Å for L = HCO_2^-; 1.817(4) Å for L = HCO_3^-).[32]

Table 1. Ni_{1s}→Ni_{3d}, S_{1s}→Ni_{3d}, S_{1s}→$S_{C\text{-}S}^{*}$ Transition Energy and S_{1s}→Ni_{3d} Transition Intensity of Complexes **1**, **2**, **4**, and $[Ni(SPh)(PS_3)]^-$ Derived from Ni and S K-edge X-ray Absorption Spectroscopy.

Complexes	Ni_{1s}→Ni_{3d}	S_{1s}→Ni_{3d} Energy (eV)[b]			S_{1s}→Ni_{3d} Intensity[b]		S_{1s}→$S_{C\text{-}S}^{*}$	Relative
	Energy (eV)[a]	1st peak	2nd peak	Avg.[c]	1st peak	2nd peak	Energy (eV)[b]	d-manifold energy shift (eV)[d]
1	8332.9	2469.7	2470.4	2470.0	0.29	1.34	2472.1	0
2	8333.1	2469.9	2470.5	2470.3	0.47	1.15	2472.1	0.3
4	8332.7	2469.5	2470.2	2470.1	0.33	1.77	2472.2	0
$[Ni(SPh)(PS_3)]^-$	8333.0	2469.8	2470.4	2470.3	0.52	1.91	2472.3	0.1

[a]The peak energy is determined by the minimum of the second derivative. [b]The peak energy and intensity is determined based on the spectral deconvolution. [c]The intensity-weighted average energy is given here. [d]Calculated from the difference of the thiolate peak energy and the intensity-weighted pre-edge peak energy.

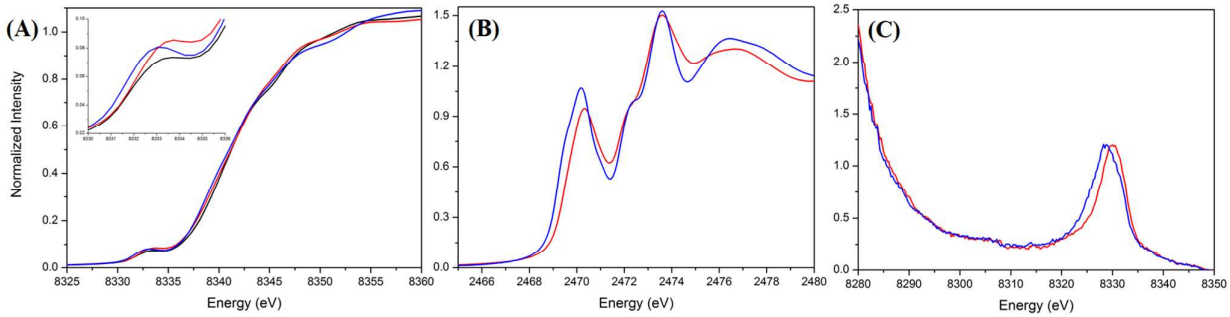

Figure 3. (**A**) Ni K-edge X-ray absorption spectra of complexes **1** (black), **2** (red), and **4** (blue). (**B**) S K-edge X-ray absorption, and (**C**) Ni valence-to-core X-ray emission spectra of complexes **2** (red) and **4** (blue).

X-ray absorption/emission spectrum

Ni and S K-edge X-ray absorption spectroscopic (XAS) study of complex **2** was further attempted to investigate its electronic structure using complexes **1** and **4** as reference complexes. As shown in Figure 3A, the Ni K-edge XAS of complex **2** (8333.1 eV) together with the analogous complexes **1** (8332.9 eV) and **4** (8332.7 eV) shows similar Ni_{1s}-to-Ni_{3d} transition energy. Accordingly, the formal oxidation state of Ni in complex **2** is similar to those of complexes **1** and **4**, which are generally known as a L ligand bound to a d^7 Ni(III) center in $[Ni^{III}(L)(PS_3)]^-$.[28] Figure 3B and SI Figure S4 depict the S K-edge XAS spectra of complexes **1**, **2**, and **4**, whereas SI Figure S5 shows the calculated S K-edge XAS spectra and spectral deconvolution. As shown in Table 1, the intensity-weighted average energy of S_{1s}-to-Ni_{3d} transitions in combination with S_{1s}-to-$S_{C\text{-}S}$* transition energy demonstrate that the Ni_{3d} manifold orbital energy of complex **2** is 0.3 eV higher than those of complexes **1** and **4**.[33-34] With further regard to the Ni_{1s}-to-Ni_{3d} pre-edge transition energy observed in the Ni K-edge XAS, Ni Z_{eff} of complexes **1**, **2**, and **4** are all comparable. That is, Ni and S K-edge XAS study supports the $[Ni^{III}:CO_2^{\bullet-}]$ electronic structure in complex **2**. As shown in Figure S6, cyclic voltammogram of 2 mM solution of complex **4** in CH_3CN indicates a reversible interconversion between Ni^{III}/Ni^{II} at $E_{1/2}$ = -0.58 V and an irreversible oxidation at E_{pa} = -0.21 V, whereas complex **2** exhibits a reversible interconversion between Ni^{III}/Ni^{II} at $E_{1/2}$ = -0.70 V and an irreversible oxidation at E_{pa} = -0.29 V (vs. Fc/Fc^+).

Regarding complex **4** as an isolobal equivalent to $[Ni^{III}:CO_2]$, complex **2** is a Ni^{III} complex bearing a 17-valence-electron $[CO_2]^{\bullet-}$ ligand. The significant lower intensity of the second S_{1s}-to-Ni_{3d} transition peak observed in the S K-edge XAS spectrum of complex **2**, compared to that of complex **4**, discloses that the one-extra electron shared by axial Ni_{3d} orbital and $2\pi_u^*$ orbital of CO_2 leads to the strengthening of the Ni^{III}-$CO_2^{\bullet-}$ bond and stabilizes the coordination of κ^1-$[CO_2]^{\bullet-}$ toward Ni^{III} center (Figure 3B and Table 1). As observed in complex $[Ni^{III}(L)(PS_3)]^-$ (L = OMe, SEt, SPh), complex **4** displays EPR silence at 300 K, an axial signal at g = 2.27 and 2.04 at 77 K, and an effective magnetic moment of 1.74 μ_B at 300 K (Figures 4C and S7A).[27-28, 35] Stabilization of $[CO_2]^{\bullet-}$ radical through coordination to the Ni^{III} center in complex **2** was further evidenced by EPR spectroscopy.

As shown in Figures 4A and 4B, the EPR spectrum of complex **2** at 77 K, apparently, resembles the combination of typical EPR signal of $[Ni^{III}(L)(PS_3)]^-$ (g = 2.31, 2.03, and 2.00) and $[CO_2]^{\bullet-}$ radical with a contribution of Ni_{3d} leading to the observed g anisotropy (Figures 4A and 4B).[36] Spin quantitation of complex **2**, using complex **4** as a reference, demonstrates that the electronic structure of complex **2** is best described as a resonance hybrid between $[Ni^{III}:CO_2^{\bullet-}]$ and

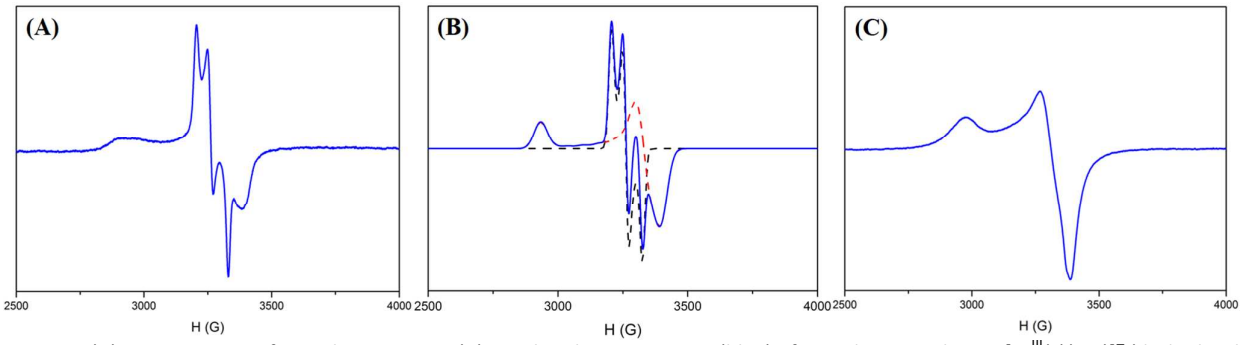

Figure 4. (**A**) EPR spectrum of complex **2** at 77 K, (**B**) simulated EPR spectrum (blue) of complex **2** combining $[Ni^{III}(L)(PS_3)]^-$ (dashed red line) and $[CO_2]^{\bullet-}$ radical (dashed black line), (**C**) EPR spectrum of complex **4** at 77 K.

$[Ni^{II}:CO_2]$, which is supported by the effective magnetic moment of 1.59 μ_B exhibited by complex **2** at 300 K (SI Figure S7B and S7C).

Experimental valence-to-core X-ray emission spectroscopy (V2C XES) spectra of complexes **2** and **4** are presented in Figure 3C. In comparison with complex **4**, the broad V2C transition peak of complex **2** at 8330.0 eV shifts from 8328.8 eV upon replacement of the $[NCO]^-$ by $[CO_2]^{\bullet-}$ ligand. DFT calculation was further pursued to verify the nature of the V2C transition(s). As shown in SI Figure S8A and S8B, DFT calculated V2C XES spectra resembles the experimental V2C features and, in particular, the trend of the energy shift comparing complexes **2** and **4**. Contribution of 4 σ_g, 3 σ_u, 1 π_g orbitals of $[NCO]^-$ and Ni_{3d}-S_{3p} orbitals results in the V2C features of complex **4**.[37] For complex **2**, the absence of transitions from 3 σ_u and 1 π_g orbitals and an additional transition from occupied 2 π_u orbital of $[CO_2]^{\bullet-}$, in addition to the upward shift of Ni_{3d}-S_{3p} orbitals in complex **2**, rationalizes the higher V2C transition energy of complex **2** in comparison with complex **4**.

Complex $[Ni(L)(P(C_6H_3\text{-}3\text{-}SiMe_3\text{-}2\text{-}S)_3)]^-$, embedded in a distorted trigonal bipyramidal geometry, features a wealth of chemical reactivity tailored by the oxidation state of Ni and coordinating ligand L (L = OPh, SPh, SePh and Cl for Ni^{III}; L = CO, N_2H_4 for Ni^{II}).[27-28, 35] To dissect the unique reactivity of $[Ni^{III}(OMe)(PS_3)]^-$ (**1**) toward CO_2 activation, addition of CO_2 into THF solution of the representive Ni^{III}-chalcogenate complex $[Ni(SPh)(PS_3)]^-$ was investigated. In contrast to the reaction of complex **1** and CO_2 yielding complex **2**, complex $[Ni^{III}(SPh)(PS_3)]^-$ is inert toward CO_2. In addition, despite the potential reduction power of Ni^{II} center in combination with the labile nature of CO or N_2H_4 ligand, neither complex $[Ni^{II}(CO)(PS_3)]^-$ nor complex $[Ni^{II}(N_2H_4)(PS_3)]^-$ shows reactivity toward CO_2 when the THF solution of these Ni complexes was treated with CO_2, respectively, at ambient temperature for 3 days. As shown in SI Figure S4 and Table 1, the covalent character of $[Ni^{III}(SPh)]$ core, compared to $[Ni^{III}(OMe)]$ core, derived from the σ-/π-electron-donating nature of the coordinated phenylthiolate ligand, rationalizes the inertness of $[Ni^{III}(SPh)(PS_3)]^-$ toward CO_2.[33-34] Despite the labile nature of CO and N_2H_4, the inert reactivity of Ni^{II} center toward CO_2 demonstrates that the lowered Ni_{3d} manifold orbitals in Ni^{III} complex **1** attracts the binding of weak σ-donor CO_2 and triggers the subsequent reduction of CO_2 by the nucleophilic $[OMe]^-$ in the immediate vicinity. Reactivity of complex **1** toward CO_2 affording an O-bound $[Ni^{III}:CO_2^{\bullet-}]$ species uncovers a novel strategy for immobilization and reductive activation of CO_2, contrary to typical interaction of unoccupied CO_2 $2\pi_u$* orbitals with filled high-lying metal d orbitals in low-valence metal complexes.[38-39] Theoretically, lowering the energy of the $2\pi_u^*(6a_1)$ (LUMO) orbital on CO_2 for interaction with nickel orbitals binding by way of O=C-unit may be responsible for the coordinated CO_2 reduction and the nonlinearity of the triatomic CO_2 molecule which contains 17 valence electrons, as reported by McGlynn and co-workers.[37] These results illustrate the aspects of how a coordinated ligand and the electronic state of nickel center work in concert to trigger coordination and activation of CO_2.

Conclusions

Complex **1**, inherent with the combination of the electrophilic $[Ni^{III}(PS_3)]$ core and the properly positioned $[OMe]^-$ nucleophile, was employed to provide an optimum electronic condition to trap and activate CO_2 to afford complex **2** containing the O-coordinated $[\kappa^1\text{-}CO_2]^{\bullet-}$ ligand. Ni^{III}-mediated reduction of CO_2 by adjacent $[OMe]^-$ ligand immobilizes CO_2 in a form of $[Ni^{III}:CO_2^{\bullet-}]$ and may open a novel CO_2 activation pathway promoting the subsequent incorporation of CO_2 in the buildup of functionalized products.

Acknowledgements

We gratefully acknowledge the support on the hardware and software from staff at BL-16A and BL-17C of NSRRC, and BL 6-2 of SLAC. Authors thank Ms. Pei-Lin Chen for single-crystal X-ray structural determinations, Mr. Yu-Huan Lu and Prof. Hsin-Tsung Chen for the help on theoretical calculation. We also thank the Ministry of Science and Technology (Taiwan) for the financial support.

Notes and References

1 T. Sakakura, J. C. Choi and H. Yasuda, *Chem. Rev.*, 2007, **107**, 2365.
2 D. J. Darensbourg, *Chem. Rev.* 2007, **107**, 2388.
3 J.-H. Jeoung, H. Dobbek, *Science*, 2007, **318**, 1461.
4 M. Can, F. A. Armstrong, S. W. Ragsdale, *Chem. Rev.*, 2014, **114**, 4149.
5 J. Fesseler, J.-H. Jeoung, H. Dobbek, *Angew. Chem.*, 2015, **54**, 8560.
6 M. Aresta, C. F. Nobile, V. G. Albano, E. Forni, M. Manassero, *J. C. S. Chem. Comm.*, 1975, 636.
7 J. S. Anderson, V. M. Iluc, G. L. Hillhouse, *Inorg. Chem.*, 2010, **49**, 10203.
8 Y.-E. Kim, J. Kim, Y. Lee, *Chem. Comm.*, 2014, **50**, 11458.
9 Y.-E. Kim, S. Oh, S. Kim, O. Kim, J. Kim, S. W. Han, Y. Lee, *J. Am. Chem. Soc.* 2015, **137**, 4280.
10 C. Costentin, M. Robert, and J. M. Saveant, *Chem. Soc. Rev.*, 2013, **42**, 2423.

11 M. Aresta and A. Dibenedetto, *Dalton Trans.*, 2007, 2975.
12 A. Looney, R. Han, K. Mcneill and G. Parkin, *J. Am. Chem. Soc.*, 1993, **115**, 4690.
13 O. R. Allen, S. J. Dalgarno, L. D. Field, P. Jensen, A. J. Turnbull and A. C. Willis, *Organometallics*, 2008, **27**, 2092.
14 A. Jana, D. Ghoshal, H. W. Roesky, I. Objartel, G. Schwab and D. Stalke, *J. Am. Chem. Soc.*, 2009, **131**, 1288.
15 S. F. Yin, J. Maruyama, T. Yamashita and S. Shimada, *Angew. Chem.*, 2008, **47**, 6590.
16 B. Kersting, *Angew. Chem.*, 2001, **40**, 3987.
17 M. Vogt, A. Nerush, Y. Diskin-Posner, Y. Ben-David, & D. Milstein, *Chem. Sci.*, 2014, **5**, 2043.
18 G. A. Filonenko, M. P. Conley, C. Copéret, M. Lutz, E. J. M. Hensen and E. A. Pidko, *ACS Catal.*, 2013, **3**, 2522.
19 C. C. Lu, C. T. Saouma, M. W. Day, and J. C. Peters, *J. Am. Chem. Soc.*, 2007, **129**, 4.
20 M. T. Whited and R. H. Grubbs, *J. Am. Chem. Soc.*, 2008, **130**, 5874.
21 B. C. Fullmer, H. J. Fan, M. Pink and K. G. Caulton, *Inorg. Chem.*, 2008, **47**, 1865.
22 I. Castro-Rodriguez and K. Meyer, *J. Am. Chem. Soc.*, 2005, **127**, 11242.
23 S. C. Bart, C. Anthon, F. W. Heinemann, E. Bill, N. M. Edelstein and K. Meyer, *J. Am. Chem. Soc.*, 2008, **130**, 12536.
24 J. G. Rebelein, Y. Hu and M. W. Ribbe, *Angew. Chem.*, 2014, **53**, 11543.
25 R. Angamuthu, P. Byers, M. Lutz, A. L. Spek and E. Bouwman, *Science*, 2010, **327**, 313.
26 G. H. Jin, C. G. Werncke, Y. Escudiee, S. Sabo-Etienne and S. Bontemps, *J. Am. Chem. Soc.*, 2015, **137**, 9563.
27 T.-W. Chiou and W.-F. Liaw, *Inorg. Chem.*, 2008, **47**, 7908.
28 C.-M. Lee, Y.-L. Chuang, C.-Y. Chiang, G.-H. Lee and W.-F. Liaw, *Inorg. Chem.*, 2006, **45**, 10895.
29 N. A. M. Azman, S. Peiro, L. Fajari, L. Julia and M. P. Almajano, *J. Agr. Food Chem.*, 2014, **62**, 5743.
30 I. Castro-Rodriguez, H. Nakai, L. N. Zakharov, A. L. Rheingold and K. A Meyer, *Science*, 2004, **305**, 1757.
31 W. J. Evans, C. A. Seibel and J. W. Ziller, *Inorg. Chem.*, 1998, **37**, 770.
32 D. G. Huang and R. H. Holm, *J. Am. Chem. Soc.*, 2010, **132**, 4693.
33 T.-T. Lu, S.-H. Lai, Y.-W. Li, I-J. Hsu, L.-Y. Jang, J.-F. Lee, I-C. Chen and W.-F. Liaw, *Inorg. Chem.*, 2011, **50**, 5396.
34 E. I. Solomon, B. Hedman, K. O. Hodgson, A. Dey and R. K. Szilagyi, *Coord. Chem. Rev.*, 2005, **249**, 97.
35 C.-M. Lee, C.-H. Chen, S.-C. Ke, G.-H. Lee and W.-F. Liaw, *J. Am. Chem. Soc.*, 2004, **126**, 8406.
36 J. H. Lunsford and J. P. Jayne, *J. Phys. Chem.*, 1965, **69**, 2182.
37 J. W. Rabalais, J. M. Mcdonald, V. Scherr and S. P. Mcglynn, *Chem. Rev.*, 1971, **71**, 73.
38 X. L. Yin and J. R. Moss, *Coord. Chem. Rev.*, 1999, **181**, 27.
39 D. H. Gibson, *Chem. Rev.*, 1996, **96**, 2063.